

# The XMM-Newton/2dF survey VII. is there any X-ray absorption in optically selected QSOs?

A. Akylas<sup>1,2</sup>, A. Georgakakis<sup>1</sup>, I. Georgantopoulos<sup>1</sup>

<sup>1</sup> *Institute of Astronomy & Astrophysics, National Observatory of Athens, I. Metaxa B. Pavlou, Penteli, 15236, Athens, Greece*

<sup>2</sup> *Physics Department University of Athens, Panepistimiopolis, Zografos, 15783, Athens, Greece*

26 October 2018

## ABSTRACT

We explore the X-ray properties of optically selected QSOs spectroscopically identified in the course of the 2dF QSO survey (2QZ). Our main goal is to expand to higher redshifts previous findings suggesting the presence of a fraction of X-ray obscured sources among the low redshift optically selected broad line AGN population. The X-ray data are from the wide field ( $\sim 2.5 \text{ deg}^2$ ) shallow [ $f(0.5 - 8 \text{ keV}) \approx \times 10^{-14} \text{ erg cm}^{-2} \text{ s}^{-1}$ ] XMM-Newton/2dF survey. A total of 96 2QZ QSOs overlap with the area covered by our X-ray survey. 66 of them have X-ray counterparts while 30 remain undetected in our X-ray survey. The 66 X-ray detected QSOs have a mean photon index of  $\approx 2$  suggesting little or no X-ray obscuration for most of these sources. Individual X-ray spectral fittings reveal only 1 source (intrinsic  $L_X(0.5 - 8 \text{ keV}) \sim 10^{44} \text{ erg s}^{-1}$  at  $z = 0.82$ ) that is likely to be obscured ( $N_H \approx 10^{23} \text{ cm}^{-2}$ ) at the 90% confidence level. Additionally, there are 9 2QZ sources that show evidence for moderate absorption (mean observed  $N_H$  of  $\approx 10^{21} \text{ cm}^{-2}$ ). For the 30 QSOs that remain undetected in our X-ray survey we use stacking analysis to estimate a mean hardness ratio of  $-0.59 \pm 0.11$  suggesting that the bulk of this population has  $N_H$  consistent with the Galactic value. However, we cannot exclude the possibility that some of these sources have enhanced photoelectric absorption that is not revealed in the mean stacked spectrum. We estimate a lower limit to the fraction of optically selected QSO with X-ray absorption of about 10% (10 out of 96).

## Key words:

Galaxies: active – quasars: general – X-rays: general

## 1 INTRODUCTION

Deep X-ray surveys in the 2–10 keV band carried out with the *Chandra* and the XMM-Newton have resolved up to 90 per cent of the hard (2–10 keV) X-ray Background (XRB) into discrete sources to a flux limit of about  $2 \times 10^{-16} \text{ erg cm}^{-2} \text{ s}^{-1}$  (Mushotzky et al. 2000; Brandt et al. 2001; Giacomoni et al. 2002). Follow-up observations have shown that the X-ray sources in these surveys are a heterogeneous mix comprising broad line QSOs, Seyfert 1 and 2 type systems, passive galaxies and optically faint sources ( $I > 24 \text{ mag}$ ) whose nature remains elusive (Alexander et al. 2001; Barger et al. 2001; Fiore et al. 2004; Georgantopoulos et al. 2004). These observations are in stark contrast to the X-ray background (XRB) population synthesis models, predicting a single dominant population of heavily obscured AGNs (Comastri et al. 1995; Fiore et al. 2004). Indeed, only a few cases of obscured (type-2; Norman et al. 2002; Stern et al.

2002) QSOs have been reported in the literature to date, suggesting revision of the population synthesis models.

To this end, there is growing evidence for a population of broad-line QSOs with little optical extinction (hence the broad optical lines) but significant X-ray absorption (Akiyama et al. 2000; Brandt, Laor & Wills al. 2000; Risaliti et al. 2001; Wilkes et al. 2002; Akylas et al. 2003). Although the apparent conflict between the optical and X-ray absorption is still poorly understood, these objects may be an important component of the X-ray background. Brandt et al. (2000) argue that about 10% of optically selected QSOs are X-ray weak at soft energies with X-ray-to-optical flux density ratios  $\alpha_{ox} > 2$ . Using the C IV UV absorption spectral feature they argue that the X-ray weakness in these systems is most likely due to absorption. Indeed, Gallagher et al. (2001) studied the X-ray spectral properties of the soft X-ray weak population using *ASCA* and *Chandra* data and found direct evidence for significant obscuring column den-

sities in excess of  $10^{22} \text{ cm}^{-2}$ . On the basis of the studies above Brandt et al. (2000) suggest that selecting soft X-ray weak galaxies ( $\alpha_{ox} > 2$ ) produces samples with a high incidence of X-ray obscured sources. However, broad line AGNs with significant X-ray absorption may be present, albeit in smaller numbers, among the  $\alpha_{ox} < 2$  population.

In this paper we address this issue by combining a homogeneous sample of optically selected QSOs with a wide area ( $2.5 \text{ deg}^2$ ) shallow ( $f_x(0.5 - 8 \text{ keV}) \approx 10^{-14} \text{ erg s}^{-1} \text{ cm}^{-2}$ ) XMM-Newton survey (Georgakakis et al. 2003, 2004). The QSO sample is compiled from the 2dF QSO survey (2QZ; Croom et al. 2001) which is based on optical/UV colour selection of sources with  $b_J < 20.85 \text{ mag}$ . This is about 4.5 mag fainter than the magnitude limit of the Bright Quasar Survey (Schmidt & Green 1983) used by Brandt et al. (2000) to explore the properties of soft X-ray weak AGNs. The main goal of our study is to expand to higher redshifts previous findings suggesting the presence of a fraction of X-ray obscured sources among the low redshift optically selected broad line AGN population, irrespective of their  $\alpha_{ox}$ , using X-ray spectral analysis. Such a population could play an important role in the XRB synthesis models as well as in unified AGN schemes.

In Section 2 we describe the X-ray and the optical data used in the present study. Section 3 outlines the X-ray data reduction while in Section 4 we present the X-ray data analysis. The results are discussed in Section 5 and our conclusions are summarized in Section 6. Throughout this paper we adopt  $H_0 = 65 \text{ km s}^{-1} \text{ Mpc}^{-1}$ ,  $\Omega_M = 0.3$  and  $\Omega_\Lambda = 0.7$ .

## 2 THE X-RAY SAMPLE

The X-ray data are from the wide field (18 pointings) bright (2-10 ks per pointing) XMM-Newton/2dF survey. The observations are carried out near the North (9 fields) and the South (9 fields) Galactic Pole regions. We have excluded from our analysis 1 northern and 4 southern XMM-Newton fields suffering from strong particle background (see Georgakakis et al. 2003, 2004). The remaining 13 fields cover a total area of  $\sim 2.5 \text{ deg}^2$  and overlap with the 2QZ survey. The 2QZ is a large-scale spectroscopic program designed to follow optically selected QSOs using the 2dF multi-fibre spectrograph on the 4-m Anglo-Australian Telescope (AAT). The complete 2dF catalogue covers a total area of  $740 \text{ deg}^2$  and comprises about 25 000 QSOs in the magnitude range  $18.25 < b_J < 20.85 \text{ mag}$ . The 2QZ spectra cover the wavelength range 3700–7900 Å. A total of 96 2QZ QSOs overlap with these fields.

The X-ray sources are detected in the 0.5-8 keV energy band using a threshold of  $5\sigma$ . We detect 521 X-ray sources in total. The cross correlation between the X-ray data and the 2QZ catalogue reveals 66 matches within a distance less than 5 arcsec. This represents about 70 per cent of the 2QZ QSOs in our fields. These optically identified Broad Line QSOs are located both in the North (33 sources) and the South (33 sources) Galactic Pole regions spanning the redshift range of  $0.5 < z < 3$ . We also use radio data from the FIRST (Faint Images of the Sky at Twenty Centimeters; Becker et al. 1995) and the NVSS (NRAO VLA Sky Survey; Condon et al. 1998) radio surveys to identify our X-ray data with radio sources. The observations are carried out at 1.4 GHz

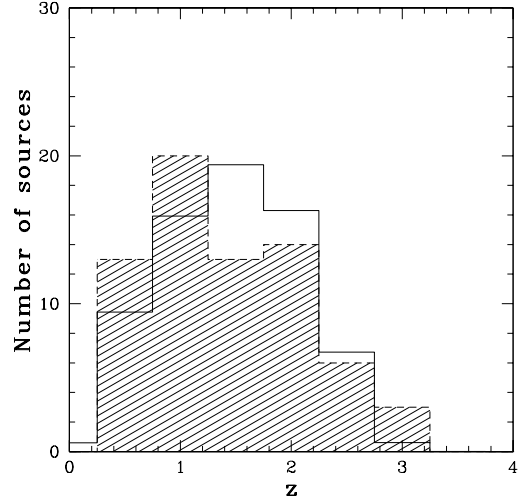


**Figure 1.** The redshift distribution of 66 optically selected QSOs (shaded histogram) in comparison with the normalized redshift distribution of the full 2QZ QSO catalogue (unshaded histogram).

with a limiting flux density of 1 and 2.5 mJy for the FIRST and the NVSS respectively. Within a 10 arcsec distance there is no coincidence of our optically selected QSOs with radio sources.

In Figure 1 we compare the redshift distribution of the 66 QSOs of our sample (shaded histogram) with that of the (normalized) full 2QZ sample. A Kolmogorov-Smirnov test suggests that the two datasets are drawn from the same parent population at the 90 per cent confidence level. The median redshift of the 2QZ QSOs with and without X-ray counterparts is 1.3 and 1.7 respectively. The mean 2500 Å luminosity density of the two populations above is estimated to be  $2.2 \times 10^{30} \text{ erg s}^{-1} \text{ Hz}^{-1}$  and  $3.4 \times 10^{30} \text{ erg s}^{-1} \text{ Hz}^{-1}$  respectively (see section 5 for details).

## 3 THE X-RAY DATA REDUCTION

The X-ray data have been obtained with the EPIC (European Photon Imaging Camera; Strüder et al. 2001 and Turner et al. 2001) cameras on board the XMM-Newton operating in full frame mode with the thin filter applied. The data have been analyzed using the Science Analysis Software (SAS 5.3). Event files for both the PN and the MOS detectors have been produced using the EPCHAIN and EMCHAIN tasks of SAS respectively. The event files were screened for high particle background periods by rejecting times with 0.5-10 keV count rates higher than 25 and 15 cts/s for the PN and the two MOS cameras respectively.

In our analysis we have dealt only with events corresponding to patterns 0-4 for the PN and 0-12 for the MOS instruments. To increase the signal-to-noise ratio and to reach fainter fluxes we have merged the PN and the MOS event files into a single event list using the MERGE task of SAS. We have extracted images and background maps in three different energy bands 0.5-8 (total), 0.5-2 (soft), and 2-8 keV (hard) for both the individual and the combined event files. Exposure maps and bad pixel masks have also been constructed in the above energy bands to take into account the

vignetting effect and the presence of hot CCD pixels and gaps between the CCDs. We use the more sensitive (higher S/N ratio) merged image for source extraction and flux estimation, while the individual PN and MOS images are used to calculate hardness ratios. This is because the interpretation of hardness ratios is simplified if the extracted count rates are from one detector only. A small fraction of sources lie close to masked regions (CCD gaps or hot pixels) on either the MOS or the PN detectors. This may introduce errors in the estimated source counts. To avoid this bias, the source count rates (and hence the hardness ratios and the flux) are estimated using the detector (MOS or PN) with no masked pixels in the vicinity of the source.

The source counts for all the images are estimated within an 18 arcsec circle area. This area includes at least 70 per cent of the X-ray source photons at off-axis angles less than 10 arcmin. The source counts are divided with the appropriate exposure time to correct for the vignetting effect. For the encircled energy correction, accounting for the energy fraction outside the aperture within which source counts are accumulated, we adopt the calibration given by the XMM-Newton Calibration Documentation<sup>\*</sup>. We convert count rates to flux assuming an absorbed power law spectrum with  $\Gamma = 1.7$  and Galactic column density  $N_H = 2 \times 10^{20} \text{ cm}^{-2}$  appropriate for these fields (Dickey & Lockman 1990). The Energy Conversion Factor (ECF) is obtained using PIMMS software v3.3a. Adopting  $\Gamma=2$  will lower our 0.5–8 keV flux estimates by 20 per cent. As discussed in section 5 this has a negligible effect in our analysis. In the case of the simultaneous detection in the mosaic image, the mean ECF is estimated by weighting the ECFs of the individual detectors using the respective exposure time.

For the X-ray spectral analysis we produce the individual spectra files using the SAS task EVSELECT. The background spectra files are extracted from every image independently, using regions free from sources. The response matrices and the auxiliary files are produced using the SAS tasks RMFGEN and ARFGEN respectively. We have used the XSPEC v11.2 software to fit the data. All the quoted errors correspond to the 90 per cent confidence level.

## 4 DATA ANALYSIS

### 4.1 Hardness ratios

In Figure 2 we plot the hardness ratio (HR) as a function of the 0.5–8 keV flux. By definition ( $HR = H-S/H+S$ , where H and S are the net counts in the 2–8 keV and 0.5–2 keV band respectively) less negative HR values suggest less soft energy (<2 keV) photons compared to the harder energies (>2 keV) in the X-ray spectra. This can be attributed to the presence of a larger column density. A total of eight sources have zero or negative net counts in the hard band. For these sources we set the HR to  $-1$ . These sources are not plotted in Figure 2. Due to the presence of bad pixels, the source counts are not always estimated from the same instrument (see section 3). In order to distinguish between the two different cases we use filled circles (42 points) and open boxes (16 points) to plot

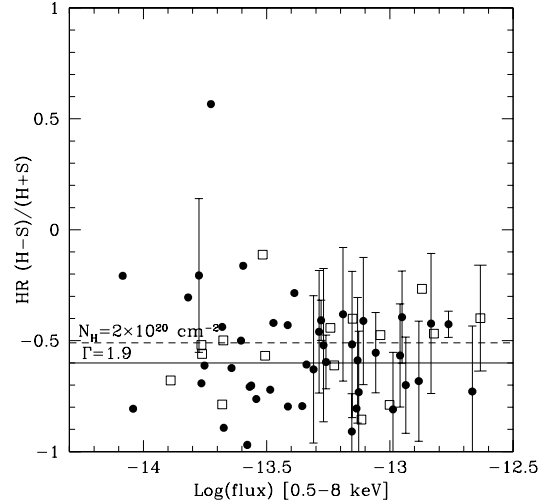


**Figure 2.** Hardness ratio against 0.5–8 keV flux. Filled circles denote the HR values obtained using the PN data, while open boxes are for HR values obtained using the MOS data. The solid and dashed lines show, respectively, the expected PN and MOS HR values for a power-law model with  $\Gamma = 1.9$  and  $N_H = 2 \times 10^{20} \text{ cm}^{-2}$ . The error bars correspond to the 90 per cent confidence level. For clarity, points with uncertainties greater than 0.35 are plotted without error bars.

the HR values obtained using the PN and MOS event files respectively. For clarity we plot the 90 per cent error bars only when they are smaller than 0.35. The two horizontal lines show the expected HR for a power-law model with  $\Gamma = 1.9$  and  $N_H = 2 \times 10^{20} \text{ cm}^{-2}$  for the PN (solid line) and the MOS (dashed line). Note that the difference between the two lines vanishes as we move toward positive HR values (i.e. higher column densities  $> 5 \times 10^{21} \text{ cm}^{-2}$ ).

In Figure 2 there is no strong evidence of obscuration. Within the 90 per cent confidence level most of the HR values are consistent with a photon index of  $\sim 1.9$ . There is only one source (#38) which shows a very flat spectrum on the basis of the HR value, albeit with large error bar ( $HR = 0.57 \pm 0.60$ ). The unweighted mean HR values for the PN and MOS data are  $\langle HR_{PN} \rangle = -0.55$  and  $\langle HR_{MOS} \rangle = -0.53$  corresponding to an observed column density of  $N_H = 5 \times 10^{20} \text{ cm}^{-2}$  for  $\Gamma = 1.9$ . The *observed* column density however, is lower than the *rest-frame* one because the *k*-correction shifts the absorption turnover to lower energies. The relation between the intrinsic rest-frame and the observed column density scales approximately as  $(1+z)^{2.65}$  (Barger et al. 2002). Using this relation the above mean hardness ratios correspond to a maximum intrinsic column density of  $N_H = 2 \times 10^{21} \text{ cm}^{-2}$  at  $z = 1$ . In Figure 3 we plot the HR as a function of redshift. There is no evidence for evolution of HR values with redshift.

### 4.2 Individual spectral fittings

We attempt to further investigate the X-ray properties of the data performing individual spectral fittings for all 66 sources. The poor count statistics do not allow the use of the standard  $\chi^2$  analysis. Instead we use the C-statistic technique (Cash 1979), which is proper for fitting spectra with

<sup>\*</sup> [http://xmm.vilspa.esa.es/external/xmm\\_sw\\_cal/calib/documentation.shtml#XRT](http://xmm.vilspa.esa.es/external/xmm_sw_cal/calib/documentation.shtml#XRT)

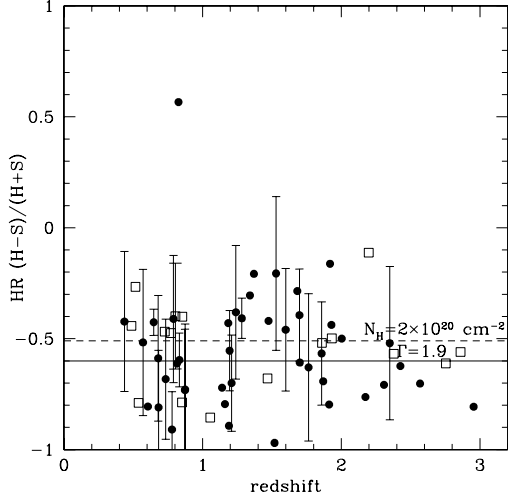


**Figure 3.** Hardness ratio against redshift. Filled circles denote the HR values obtained using the PN data, while open boxes are for HR values obtained using the MOS data. The solid and dashed lines show respectively the expected PN and MOS HR values for a power law model with  $\Gamma = 1.9$  and  $N_H = 2 \times 10^{20} \text{ cm}^{-2}$ . The error bars correspond to the 90 per cent confidence level. For clarity, points with uncertainties greater than 0.35 are plotted without error bars.

limited number of counts. Note that this method can be used to estimate parameter values and confidence regions but does not provide a goodness-of-fit (see Arnaud, George & Tennant 1992). We fit simultaneously the PN and the MOS data for each source in the energy range 0.2–8 keV. Due to the presence of hot pixels and CCD gaps, especially in the PN detector, and because of a small offset between the PN and the MOS field of view, we are able to extract spectra from both the PN and the MOS detectors for 44 sources. There are 16 sources with MOS spectra only and 6 sources with PN spectra only.

We use an absorbed power law model to fit the data. First we fix the photon index to 1.9 and allow both the  $N_H$  and the normalization to vary. The results are presented in Table 1. There are only three sources (#2, #22, #56) which appear to have a column density above the Galactic one ( $2 \times 10^{20} \text{ cm}^{-2}$ ). All the other  $N_H$  values are fully consistent with the Galactic value within the 90 per cent confidence level. In this case the  $N_H$  values listed in Table 1 correspond to the 90 per cent upper limit. We also try to fit the data using an absorbed power law model with the  $N_H$  fixed to the Galactic value while the photon index and the normalization are free parameters. In this case a flat photon index is an indication of obscuration. There is a strong evidence for obscuration only in one case (source #22). There are also nine sources (see Table 1) which may be obscured on the basis of their photon index value. For these sources we find a flat photon index,  $< 1.6$ . We note however, that within the 90 per cent uncertainties the estimated  $\Gamma$ s are consistent with 1.9.

### 4.3 Average spectra

Here we examine the average X-ray properties of our sample. First we construct three merged datasets adding respectively

**Table 2.** Average PN and MOS spectral fitting results for all the sources in our sample.

Sample	$N_H (\times 10^{20} \text{ cm}^{-2})$	$\Gamma$	$\chi^2/\text{dof}$
<sup>1</sup> PN	$< 1.1$	$2.00^{+0.11}_{-0.06}$	146.7/115
<sup>2</sup> MOS	$< 1.8$	$2.07^{+0.10}_{-0.07}$	163.7/146
PN+MOS	$< 1.1$	$2.05^{+0.07}_{-0.06}$	313.87/263

<sup>1</sup> 51 sources

<sup>2</sup> 61 sources

the individual PN (50), MOS1 (60) and MOS2 (60) spectral files, using the ftool task MATHPHA. These files are binned to give a minimum of 20 counts per bin so that Gaussian statistics can be applied. We also use ADDARF task in FTOOLS to create an average auxiliary file for each merged dataset. Since there are no differences in the response matrices between the different CCDs we use one individual response matrix for each merged dataset. Then we fit the PN and the MOS data with an absorbed power law model. The merged spectral files for the PN and the MOS detectors do not contain the same number of sources so we first apply the model to the PN and the MOS spectral files separately. For comparison we also simultaneously fit the PN and MOS data ( $\Gamma$  and  $N_H$  parameters for the PN and the MOS are tied) allowing the normalization parameters for the PN and the MOS to vary. We present the results in Table 2. Despite the different number of sources included in each of these subsamples the results are in good agreement. In Figure 4 we plot the average spectrum, the best joint fit model and the residuals for the PN (top line), the MOS1 and the MOS2 (bottom lines) spectral files.

X-ray background studies (e.g. Tozzi et al. 2001; Stern et al. 2002), have revealed a progressive hardening of the average photon index of the X-ray sources at lower fluxes. This result has direct implication to the X-ray background synthesis models (Comastri et al. 1995). Here, we try to investigate this issue using our homogeneous selected sample of UVX QSOs. We divide the data into two subsamples according to their flux. Sources with flux greater than  $10^{-13} \text{ erg cm}^{-2} \text{ s}^{-1}$  constitute the bright sample and the remaining sources the faint sample. We use the same model to simultaneously fit the PN and the MOS data. The best-fit parameters for the bright and the faint subsamples are  $\Gamma = 2.07^{+0.08}_{-0.06}$ ,  $N_H < 0.7 \times 10^{20} \text{ cm}^{-2}$  and  $\Gamma = 2.00^{+0.12}_{-0.09}$ ,  $N_H < 2.1 \times 10^{20} \text{ cm}^{-2}$  respectively. At the fluxes probed here there is no evidence for a change of the photon index. The above results clearly show that on average the presence of obscuration in our data is not important. However there are ten sources which present a hard photon index ( $< 1.6$ ). The average photon index of these sources is  $\Gamma = 1.50^{+0.20}_{-0.20}$ . Despite the large uncertainties, this result may suggest the presence of a significant column density in these QSOs.

We have also divided the data into four subsamples based on the redshift. For this separation we adopt the following redshift intervals:  $z < 0.8$ ,  $0.8 < z < 1.2$ ,  $1.2 < z < 1.8$  and  $z > 1.8$ . These subsamples contain 16, 15, 16 and 22 sources respectively. We simultaneously fit the PN and the MOS data for each subsample applying a power law model. Figure 5 plots the average  $\Gamma$  values at the mean redshift of each

**Table 1.** Spectral fitting results for 66 X-ray detected 2QZ QSOs

No	NAME	RA (J2000)	DEC (J2000)	$^1f_{\chi} (\times 10^{-14})$ erg cm $^{-2}$ s $^{-1}$	z	$^2N_{\text{H}} (\times 10^{22})$ cm $^{-2}$	$^3\Gamma$	$^4\text{DETECTOR}$
1	J005943.9-273831	+00:59:44.0	-27:38:33	4.59	1.70	< 0.048	2.07 $^{+0.43}_{-0.40}$	PN+MOS
2	J005929.4-274339	+00:59:29.3	-27:43:42	8.76	1.19	0.094 $^{+0.086}_{-0.049}$	1.42 $^{+0.28}_{-0.26}$	PN+MOS
3	J005913.8-280652	+00:59:13.9	-28:06:54	1.77	0.81	< 0.150	1.88 $^{+0.50}_{-0.46}$	PN+MOS
4	J005903.5-275311	+00:59:03.6	-27:53:10	0.91	2.95	< 0.046	2.90 $^{+0.89}_{-0.74}$	PN
5	J005900.7-273108	+00:59:00.7	-27:31:09	10.3	0.68	< 0.003	2.76 $^{+0.12}_{-0.20}$	PN+MOS
6	J005859.1-273038	+00:58:59.1	-27:30:40	2.74	2.56	< 0.095	1.70 $^{+0.37}_{-0.40}$	PN+MOS
7	J005858.5-280319	+00:58:58.5	-28:03:21	1.68	1.53	< 0.020	2.10 $^{+0.31}_{-0.40}$	PN+MOS
8	J005855.0-273141	+00:58:55.1	-27:31:41	4.41	1.16	< 0.188	2.31 $^{+0.23}_{-0.33}$	PN+MOS
9	J005850.8-280547	+00:58:50.8	-28:05:48	5.51	0.83	< 0.038	1.97 $^{+0.44}_{-0.25}$	PN
10	J005843.7-273459	+00:58:43.7	-27:34:58	3.37	1.47	< 0.019	2.21 $^{+0.37}_{-0.34}$	PN+MOS
11	J005836.1-273820	+00:58:35.9	-27:38:21	2.12	1.19	< 0.062	1.95 $^{+0.41}_{-0.56}$	PN+MOS
12	J005831.5-273757	+00:58:31.4	-27:37:55	1.73	2.86	< 0.200	2.29 $^{+1.26}_{-0.93}$	MOS
13	J005811.4-272636	+00:58:11.8	-27:26:31	2.11	2.48	< 0.016	1.05 $^{+1.14}_{-0.94}$	PN+MOS
14	J005810.8-280817	+00:58:10.7	-28:08:21	2.09	1.92	< 0.120	2.34 $^{+1.49}_{-1.00}$	PN+MOS
15	J005805.7-275005	+00:58:05.8	-27:50:06	5.74	0.48	< 0.130	1.87 $^{+0.68}_{-0.62}$	MOS
16	J005803.3-281211	+00:58:03.5	-28:12:15	17.3	0.64	< 0.014	2.18 $^{+0.21}_{-0.28}$	PN
17	J005747.5-275412	+00:57:47.5	-27:54:10	5.26	1.28	< 0.020	1.95 $^{+0.57}_{-0.50}$	PN
18	J005740.1-282311	+00:57:40.0	-28:23:15	7.32	0.60	< 0.070	2.18 $^{+0.27}_{-0.25}$	PN+MOS
19	J005734.9-272828	+00:57:34.9	-27:28:29	2.87	2.17	< 0.100	2.01 $^{+0.57}_{-0.62}$	PN+MOS
20	J005727.9-283107	+00:57:27.9	-28:31:09	7.06	0.85	< 0.035	2.16 $^{+0.40}_{-0.37}$	MOS
21	J005724.4-273201	+00:57:24.4	-27:32:02	11.6	1.20	< 0.010	2.33 $^{+0.11}_{-0.22}$	PN+MOS
22	J005701.1-272800	+00:57:01.0	-27:28:02	1.88	0.82	2.55 $^{+1.69}_{-1.38}$	0.20 $^{+0.48}_{-0.77}$	PN+MOS
23	J005650.9-280955	+00:56:50.9	-28:9:56	9.15	0.77	< 0.095	1.75 $^{+0.47}_{-0.45}$	MOS
24	J005648.9-282158	+00:56:49.0	-28:22:01	2.70	2.30	< 0.065	2.00 $^{+0.37}_{-0.34}$	PN+MOS
25	J005634.8-281622	+00:56:34.7	-28:16:22	2.11	1.93	< 0.048	2.67 $^{+1.00}_{-0.79}$	MOS
26	J005612.4-275711	+00:56:12.4	-27:57:12	15.1	0.72	< 0.030	2.03 $^{+0.20}_{-0.25}$	MOS
27	J005602.1-282658	+00:56:02.2	-28:27:02	3.86	1.91	< 0.060	2.69 $^{+0.94}_{-0.80}$	PN+MOS
28	J005549.3-280334	+00:55:49.2	-28:03:39	2.55	1.01	< 0.033	2.40 $^{+0.32}_{-0.62}$	PN+MOS
29	J005545.2-275734	+00:55:45.1	-27:57:37	11.0	1.85	< 0.035	1.95 $^{+0.15}_{-0.17}$	PN+MOS
30	J005543.2-280457	+00:55:43.0	-28:04:58	7.48	0.87	< 0.048	1.99 $^{+0.23}_{-0.24}$	PN+MOS
31	J005504.2-280732	+00:55:04.1	-28:07:32	5.38	2.35	< 0.020	2.31 $^{+0.30}_{-0.34}$	PN+MOS
32	J005459.1-281430	+00:54:58.7	-28:14:31	7.01	0.77	< 0.057	2.21 $^{+0.56}_{-0.50}$	PN
33	J005449.6-281125	+00:54:49.2	-28:11:25	3.76	0.57	< 0.034	1.55 $^{+0.53}_{-0.65}$	PN+MOS
34	J134512.3-003132	+13:45:12.3	-00:31:31	4.10	1.68	< 0.070	1.89 $^{+0.37}_{-0.52}$	PN+MOS
35	J134455.8-000116	+13:44:55.8	-00:01:16	3.05	2.19	< 0.310	1.34 $^{+0.55}_{-0.83}$	MOS
36	J134454.6-001908	+13:44:54.9	-00:19:08	2.09	0.85	< 0.066	2.18 $^{+0.53}_{-0.50}$	MOS
37	J134437.0+003054	+13:44:37.1	+00:30:56	2.64	1.51	< 0.045	2.30 $^{+0.58}_{-0.43}$	PN+MOS
38	J134427.9-003029	+13:44:28.0	-00:30:32	0.83	1.37	< 1.600	1.40 $^{+1.45}_{-1.29}$	PN+MOS
39	J134424.5-000617	+13:44:24.8	-00:06:15	2.49	2.00	< 0.035	2.20 $^{+0.62}_{-0.67}$	PN+MOS
40	J134420.8+000226	+13:44:21.0	+00:02:29	1.72	1.87	< 0.055	2.08 $^{+0.57}_{-0.50}$	PN+MOS
41	J134420.0-003111	+13:44:20.1	-00:31:11	7.40	0.68	< 0.031	1.96 $^{+0.20}_{-0.27}$	PN+MOS
42	J134414.0-002950	+13:44:14.2	-00:29:52	9.97	0.53	< 0.004	2.89 $^{+0.27}_{-0.27}$	MOS
43	J134353.4-000520	+13:43:53.5	-00:05:18	3.27	1.14	< 0.290	1.52 $^{+0.43}_{-0.69}$	PN+MOS
44	J134347.5-002336	+13:43:47.6	-00:23:40	7.67	1.05	< 0.010	2.72 $^{+0.68}_{-0.58}$	MOS
45	J134339.6+002937	+13:43:40.0	+00:29:34	3.12	2.37	< 0.021	1.88 $^{+0.72}_{-0.74}$	MOS
46	J134331.4+001108	+13:43:31.4	+00:11:10	10.1	1.28	< 0.033	2.50 $^{+0.94}_{-0.72}$	PN+MOS

bin. The solid line corresponds to  $\Gamma = 1.9$ . There is no evidence for a trend of the spectral slope with redshift in agreement with Figure 3. All the average values are consistent with the mean slope of unobscured local AGNs ( $\Gamma \sim 1.9$ , e.g. Nandra & Pounds, 1994) at the 90 per cent confidence level. This result confirms previous findings (e.g. Vignali et al. 2003b, Piconcelli et al. 2003) suggesting that the accretion mechanism in radio quiet QSOs is the same at any redshift. We also note that the presence of a reflection com-

ponent should significantly flatten the average spectrum of QSOs above  $z=2$  (see Akiyama et al. 2000). However the existence of this component at the luminosities probed here ( $\bar{L}_X(0.5-8 \text{ keV}) = 8 \times 10^{44} \text{ erg s}^{-1}$  for  $\bar{z}=2.2$ ) is not seen.

**Table 1** – *continued*

No	NAME	RA (J2000)	DEC (J2000)	$^1 f_{\chi} (\times 10^{-14})$ erg cm $^{-2}$ s $^{-1}$	z	$^2 N_{\text{H}} (\times 10^{22})$ cm $^{-2}$	$^3 \Gamma$	$^4 \text{DETECTOR}$
47	J134324.2-002030	+13:43:24.2	-00:20:29	2.19	1.89	< 0.024	$2.90^{+3.32}_{-1.20}$	PN
48	J134323.6+001222	+13:43:23.8	+00:12:21	21.6	0.87	< 0.031	$2.06^{+0.14}_{-0.31}$	PN+MOS
49	J134314.8+002528	+13:43:14.9	+00:25:29	1.29	1.46	< 0.033	$1.95^{+1.04}_{-0.77}$	MOS
50	J134301.5-002951	+13:43:01.6	-00:29:51	0.91	2.06	< 1.000	$2.80^{+0.69}_{-1.50}$	PN+MOS
51	J134256.5+000056	+13:42:56.6	+00:00:57	23.3	0.80	< 0.048	$1.81^{+0.15}_{-0.18}$	MOS
52	J134255.4+000634	+13:42:55.4	+00:06:36	14.7	0.43	< 0.052	$2.07^{+0.73}_{-0.25}$	PN+MOS
53	J134233.7-001148	+13:42:33.7	-00:11:49	13.5	0.51	< 0.150	$1.84^{+0.60}_{-0.54}$	MOS
54	J134232.9-001551	+13:42:33.0	-00:15:50	2.78	2.13	< 0.460	$1.60^{+0.75}_{-0.67}$	PN+MOS
55	J134219.1+000254	+13:42:19.1	+00:02:56	3.85	1.18	< 0.150	$1.86^{+0.95}_{-0.85}$	PN+MOS
56	J134211.9+002950	+13:42:12.0	+00:29:50	7.03	0.57	$0.087^{+0.083}_{-0.062}$	$1.51^{+0.29}_{-0.29}$	PN+MOS
57	J134156.8+003009	+13:41:56.9	+00:30:10	6.46	1.24	< 0.046	$1.94^{+0.25}_{-0.28}$	PN+MOS
58	J134155.7-002233	+13:41:55.9	-00:22:34	2.28	2.42	< 0.058	$1.97^{+0.62}_{-0.58}$	PN+MOS
59	J134142.8+001238	+13:41:42.9	+00:12:39	7.81	0.79	< 0.100	$1.80^{+0.30}_{-0.30}$	PN+MOS
60	J134133.6-002704	+13:41:33.8	-00:27:03	1.52	1.34	< 0.400	$1.30^{+0.81}_{-0.69}$	PN+MOS
61	J134127.9+003211	+13:41:27.8	+00:32:13	4.90	1.76	< 0.070	$1.95^{+0.20}_{-0.40}$	PN+MOS
62	J134127.1+001413	+13:41:27.2	+00:14:14	11.2	1.69	< 0.024	$2.05^{+0.15}_{-0.23}$	PN+MOS
63	J134122.8-002246	+13:41:22.8	-00:22:43	2.54	1.91	< 0.060	$1.98^{+0.41}_{-0.46}$	PN+MOS
64	J134121.3-001353	+13:41:21.6	-00:13:51	13.1	0.73	< 0.004	$2.66^{+0.20}_{-0.25}$	PN+MOS
65	J134059.1-001945	+13:40:59.3	-00:19:45	1.72	1.86	< 0.140	$2.01^{+1.09}_{-0.81}$	MOS
66	J134041.4-001727	+13:40:41.6	-00:17:24	5.95	2.75	< 0.095	$1.87^{+0.50}_{-0.61}$	MOS

<sup>1</sup> X-ray flux in the 0.5-8 keV band assuming a power law model with  $\Gamma=1.7$  absorbed by a column density of  $2 \times 10^{20}$  cm $^{-2}$

<sup>2</sup> These values are obtained using an absorbed power law model with  $\Gamma$  fixed to 1.9.

<sup>3</sup> These values are obtained using an absorbed power law model with  $N_{\text{H}}$  fixed to  $2 \times 10^{20}$  cm $^{-2}$

<sup>4</sup> The detector from which we have extracted the spectral files

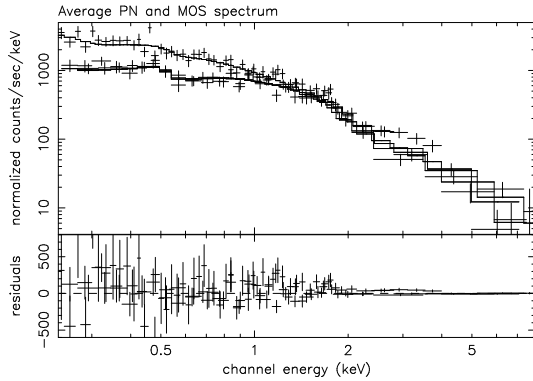


**Figure 4.** The average (0.2-8.0 keV) spectrum, the best joint fit model and the residuals for the PN (top line) and the MOS (bottom lines) sources.

## 5 DISCUSSION

We first attempt to identify obscured 2QZ QSOs using X-ray spectral fitting analysis. Using the C-statistic and assuming a power-law model with  $\Gamma = 1.9$  we find evidence for obscuration above the 90 per cent level in three sources (#2, #22 and #56). Using a flatter photon index,  $\Gamma = 1.7$ , only one source (#22) remains significantly absorbed at the 90 per cent confidence level. The rest frame column density of this object is estimated to be  $N_{\text{H}} = 12.9^{+8.5}_{-7.0} \times 10^{22}$  cm $^{-2}$  at  $z = 0.82$ . In Figure 6, plotting the (not calibrated in flux) 2QZ optical spectrum of this source, there is evidence for an absorption line at  $\sim 4800$  Å. Assuming this feature is intrinsic to the QSO this is then consistent with Mg II absorp-

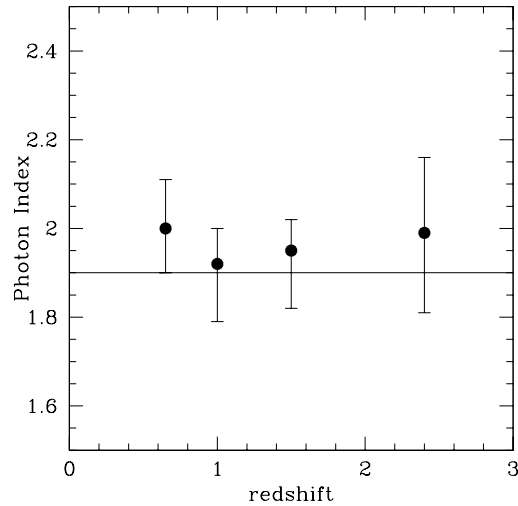


**Figure 5.** The average photon index versus mean redshift for the four redshift bins. The estimated average values are consistent with 1.9 (solid line).

tion at an outflow velocity of  $\sim 30\,000$  km/s. This absorption line, if real, may be directly associated with the material responsible for the X-ray absorption (e.g. Brandt et al. 2000). We note that the strong Mg II absorption feature of source #38 may indicate a low-ionization BAL QSO. This class of sources is believed to have high column densities associated with Compton-thick AGNs (Gallagher et al. 2002).

Furthermore, within our sample there are another nine

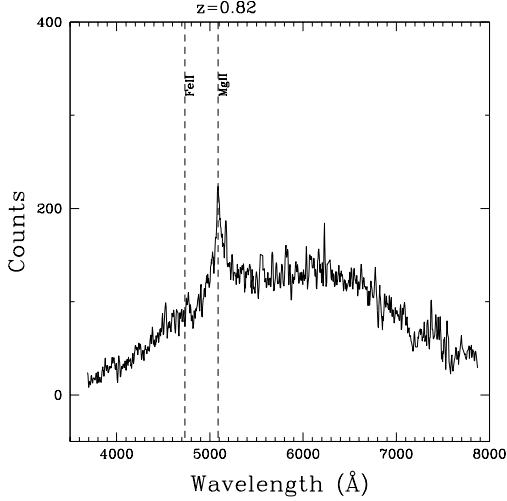


**Figure 6.** The 2DF optical spectrum (not calibrated in flux) of the absorbed QSO (#22)

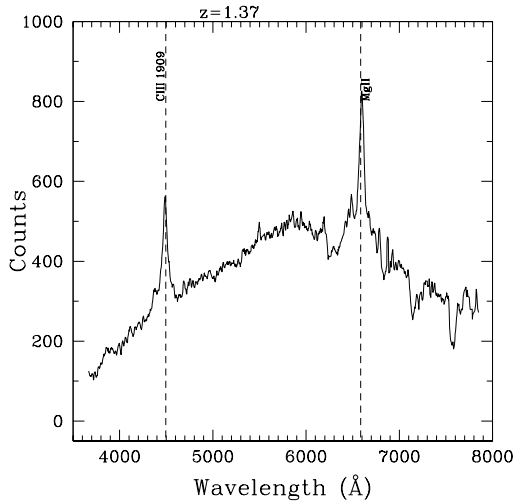


**Figure 7.** The 2DF optical spectrum (not calibrated in flux), of source #38 which presents  $\alpha_{ox} > 2$

sources which although may not show significant amount of absorption above the 90 per cent confidence level, their best fit value of  $\Gamma$  is quite hard,  $\Gamma < 1.6$  (but see note in section 4.2). The average spectrum of these sources is estimated  $\Gamma = 1.5^{+0.20}_{-0.20}$ , significantly flatter than  $\Gamma = 1.9$  suggesting absorption. The above photon index corresponds to an observed column density of  $\sim 10^{21} \text{ cm}^{-2}$ . Given that the redshift distribution of these sources is between 0.5 and 2.5 the above rest frame column density, if real, could be higher. These sources comprise about 10 per cent of our 2QZ sample.

It might be possible that the above 2QZ sources are associated with radio loud QSOs. Indeed radio loud QSOs tend to have either intrinsically flatter photon indices or enhanced photoelectric column densities (Elvis et al. 1993; Reeves & Turner 2000). As already discussed in section 2, the sources above do not have radio counterparts to the

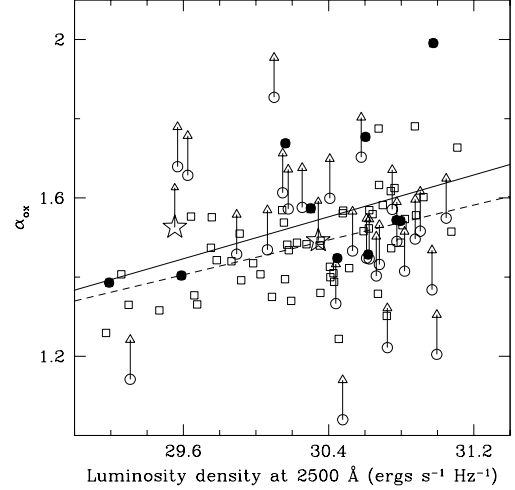


**Figure 8.** The two point optical/X-ray index,  $\alpha_{ox}$ , against 2500 Å luminosity density for the 96 2QZ QSOs. The 30 X-ray undetected QSOs are shown as lower limits. The stars are BAL QSOs on the basis of the 2QZ classification scheme. The filled circles denote the X-ray detected QSOs with a flat ( $< 1.6$ ) best fit power law photon index and the open squares shows the 66 X-ray detected QSOs. The solid line corresponds to our best linear fit to the data. The dashed line is the best fit model presented by Vignali et al. (2003a).

limits of the FIRST or the NVSS surveys. However for the optical magnitude  $b_j > 18.25$  (i.e. 2QZ selection) the radio loud/quiet boundary lies below the flux density limits of both the FIRST and the NVSS surveys (Brinkmann et al. 2000). It is therefore possible that some of the X-ray detected sources that show evidence for absorption are associated with radio loud AGN with radio flux densities below the FIRST and the NVSS limits.

We also estimate the average photon index of the 66 2QZ QSOs with X-ray counterparts and find  $\Gamma = 2.05^{+0.07}_{-0.06}$ . There is no evidence for evolution of the photon index either with redshift (see Figure 5) or flux (see section 4.3). With the exception of the sources discussed above this suggests that, on average, the X-ray absorption is not important in the sample of X-ray detected QSOs.

In addition to X-ray spectral fitting we further explore the X-ray absorption within our sample using the two point optical/X-ray spectral index,  $\alpha_{ox}$ . Following Green et al. (1995), we define  $\alpha_{ox} = 0.383 \log(f_{2500}/f_{2 \text{ keV}})$ , where  $f_{2500}$  and  $f_{2 \text{ keV}}$  are the rest frame flux densities at 2500 Å and 2 keV respectively. We calculate  $f_{2500}$  from the  $U$ -band magnitudes assuming a power-law optical spectral energy distribution of the form  $f_\nu \propto \nu^{-0.5}$ . The  $f_{2 \text{ keV}}$  is estimated from the 0.5-8 keV flux assuming a photon index  $\Gamma = 1.7$ . Adopting for the flux estimation  $\Gamma=2$  results in a negligible change in  $\alpha_{ox}$  of  $\sim 0.02$  for a source at  $z=2$ . A high value of  $\alpha_{ox}$  suggests a low X-ray flux relative to the optical flux. As discussed by Brandt et al. (2000) the  $\alpha_{ox}$  can reveal soft-X-ray-weak candidates that are believed to be associated with enhanced photoelectric absorption. In Figure 8 we plot the  $\alpha_{ox}$  index versus 2500 Å luminosity density ( $L_{2500}$ ). Both X-ray detected QSOs and 2QZ sources without X-ray counterparts are plotted. For the latter the  $3\sigma$  upper limits in

the X-ray flux are used. On the whole, the data do not suggest the presence of an X-ray weak and optically bright QSO population. The range of  $\alpha_{ox}$  values in Figure 8 is consistent with that expected for optically selected QSOs (Green et al. 1995).

Most previous studies suggest that the  $a_{ox}$  depends on 2500 Å luminosity (see Vignali et al. 2003a and references therein). We further explore this issue using our homogeneously selected QSO sample. To take into account the lower limits in  $a_{ox}$  we employ the *ASURV* software package Rev 1.2 (LaValley, Isobe, & Feigelson 1992), which implements the survival analysis methods presented in Feigelson & Nelson (1985) and Isobe, Feigelson & Nelson (1986). We use the Spearman rank order correlation test and the EM (Estimate and Maximize) regression algorithm. These statistical tests show that there is a strong correlation between  $a_{ox}$  and  $L_{2500}$  at the  $4\sigma$  confidence level. The slope of the best linear fit is  $0.132 \pm 0.03$  and the constant equals  $-2.46 \pm 0.93$ . These best fit parameters are in agreement with those of Vignali et al. (2003a) within the  $1\sigma$  standard deviation error. In Figure 8 we plot our best linear fit (solid line) and that derived by Vignali et al. 2003a (dashed line).

Only one source (#38 in Table 1) has  $\alpha_{ox} \approx 2$  and therefore could be significantly X-ray obscured. Unfortunately, the poor photon statistics (38 counts) do not allow us to firmly establish whether this source is obscured. The optical spectrum (not calibrated in flux) of this source however, presented in Figure 7, shows a broad absorption feature at  $\sim 6200$  Å. This can be interpreted as the Mg II absorption line at an outflow velocity of  $\sim 30\,000$  km/s that may be directly associated with any X-ray absorbing material. Brandt et al. (2000) found a strong correlation between the equivalent width of the C IV absorption line and the X-ray weakness measured by the  $\alpha_{ox}$  index. They argue that the X-ray weakness in their sample is due to photoelectric X-ray obscuration with the absorbing medium also responsible for the absorption features in the ultraviolet such as the C IV. Unfortunately, the 2QZ spectral window does not include the C IV line to directly compare our source with the Brandt et al. (2000) results. It is surprising however, that we do not find strong evidence for X-ray absorption in this source.

From the sources that show evidence for X-ray obscuration or flat X-ray spectra only 3 (#22, 38, 60) have  $\alpha_{ox} > 1.7$  suggesting enhanced (but not extreme) absorption (Brandt et al. 2000; Gallagher et al. 2001). The evidence above indicates that the  $\alpha_{ox}$  index does not reveal *all* the obscured AGN candidates. This can be attributed to: (i) X-ray flux variations affecting the estimated  $\alpha_{ox}$  index (an increase in the X-ray flux by a factor of 3 results in a reduction of  $\alpha_{ox}$  by  $\sim 0.18$ ), (ii) distinct X-ray and UV/optical absorber (Gallagher et al. 2004), (iii) the relative insensitivity of 2 keV photons to column densities lower than  $10^{22}$  cm $^{-2}$ . In the case of our high redshift ( $z > 0.5$ ) QSOs the latter is a particularly plausible scenario even for larger column densities due to the k-correction (see section 4.1).

In addition to X-ray detections, 30 sources in our sample (about 30 per cent of 2QZ QSOs) remain undetected in our X-ray survey and are plotted as lower limits in Figure 8. Some of these sources remain undetected because either they are at high redshifts and hence, too X-ray faint for the survey limit or lie at large off-axis angles from an XMM-Newton pointing centre where the sensitivity is reduced. In-

deed, the fraction of undetected sources drops to 17 per cent for 2QZ QSOs at  $z < 2$  and off-axis angles  $< 12$  arcmin. Nevertheless, the X-ray undetected 2QZ population may also comprise X-ray absorbed systems. We attempt to constrain the X-ray spectral properties of these sources using stacking analysis to estimate a mean hardness ratio of  $-0.59 \pm 0.11$  (using MOS data) corresponding to a low mean observed column density of about  $5 \times 10^{20}$  cm $^{-2}$ . Although this result suggests that most of the X-ray undetected QSOs are not significantly obscured we cannot exclude the possibility that some of them have enhanced photoelectric absorption that is not revealed in the stacked spectrum. Indeed, among the X-ray undetected 2QZ QSOs there are two sources classified as Broad Absorption Line (BAL) QSOs (see Figure 8). This class of QSOs are weak in both the soft and the hard X-ray bands with respect to their optical light (Brandt et al. 2000; Gallagher et al. 2001; Green et al. 2001). This is suggested to be due to a large column of absorbing gas ( $\sim 10^{23}$  cm $^{-2}$ ) rather than their intrinsic SED. The two BAL QSOs in our sample remain undetected in our X-ray survey, while the  $3\sigma$  upper limits in their flux do not provide strong constraints in their  $\alpha_{ox}$  index.

It is worth noting that the fraction of BAL QSOs in our sample (both X-ray detected and undetected sources) is very low (about 2 per cent). A similarly low fraction of BAL systems is found in the full 2QZ catalogue. Hewett & Foltz (2003) showed that the fraction of BAL QSOs is doubled when considering selection effects such as the optical flux lost due to absorption. Taking these effects into account they found that BAL QSOs represent about 20 per cent of optically selected QSOs. Also BAL QSOs are, on average, redder than UVX selected QSOs and therefore easily missed by UVX studies (Reichard et al. 2003). The evidence above suggests that the 2QZ survey might be biased against finding BAL QSOs. We also note that the fraction of BAL QSOs in the 2QZ survey increases (4 per cent), when considering only the high redshift QSOs since the C IV absorption line (primarily used to identify BAL QSOs) is entering the 2QZ spectral window only at high redshifts,  $z > 2$ . It is possible that a fraction of the 2QZ QSOs in the present sample (most likely those with evidence for X-ray obscuration or without X-ray counterparts) may be associated with BAL systems.

Our analysis suggests that about 10% of the X-ray detected QSOs (10 out of 96) show evidence for X-ray absorption. This is a lower limit to the fraction of optically selected QSOs with X-ray absorption since some of the X-ray undetected 2QZ sources are likely to be absorbed. This number however, is expected to be small as suggested by the soft stacked X-ray spectrum of the 30 X-ray undetected systems. The above result is consistent with that derived by Brandt et al. (2000). They found the percentage of the low-redshift ( $z < 0.5$ ) soft X-ray weak QSOs in the optically selected QSOs population to be 11%. Here we have extended this result to significantly higher redshifts. We note that this fraction does not include all the obscured broad line QSOs. For example recent studies suggest the presence of a reddened X-ray absorbed broad line QSO population (Wilkes et al. 2002; Risaliti et al. 2001). These objects have red optical colours and are therefore missed from optically selected samples like the 2QZ.



## 6 CONCLUSIONS

We explore the X-ray properties of 2QZ QSOs using data from a wide field ( $\approx 2.5 \text{ deg}^2$ ), shallow [ $f(0.5 - 8 \text{ keV}) \approx 10^{-14} \text{ erg cm}^{-2} \text{ s}^{-1}$ ] XMM-Newton survey.

The average photon index of the 66 X-ray detected QSOs is  $\sim 2$  suggesting that, on average, absorption effects are not important in this population. On the basis of individual X-ray spectral fittings there is evidence for significant obscuration in only one X-ray detected optically selected QSO. This source shows an intrinsic rest frame column density of  $N_{\text{H}} = 12.9^{+8.5}_{-7.0} \times 10^{22} \text{ cm}^{-2}$ . Additionally, a small number (total of 9) of optically selected QSOs have X-ray spectral properties suggesting moderate absorption ( $N_{\text{H}} \approx 10^{21} \text{ cm}^{-2}$ ). This population may be associated with radio loud and/or BAL QSOs. Our analysis suggests a lower limit to the fraction of optically selected QSO with X-ray absorption of about 10% (10 out of 96).

However, about 30 per cent of the 2QZ QSOs remain undetected in our X-ray survey. Although the mean X-ray spectral properties (using stacking analysis) are consistent with a Galactic value of the average column density, we cannot exclude the possibility that some of these sources are absorbed.

## 7 ACKNOWLEDGMENTS

We thank the anonymous referee for valuable comments and suggestions. This work is funded by the European Union and the Greek Ministry of Development in the framework of the Programme 'Competitiveness - Promotion of Excellence in Technological Development and Research - Action 3.3.1', Project 'X-ray Astrophysics with ESA's mission XMM', MIS-64564. The 2dF QSO Redshift Survey (2QZ) was compiled by the 2QZ survey team from observations made with the 2-degree Field on the Anglo-Australian Telescope.

## REFERENCES

- Akiyama, M., et al., 2000, 532, 700  
 Akylas, A., Georgantopoulos, I., Barcons, X., 2003, A&A, 403, 869  
 Alexander, D. M., et al., 2001, AJ, 122, 2156  
 Arnaud, K. A., George, I.M., Tennant, A.F., 1992, Legacy, 2, 65  
 Barger, A. J., Cowie, L. L., Mushotzky, R. F., Richards, E. A., 2001, AJ, 121, 662  
 Barger, A. J., Cowie, L. L., Brandt, W. N., Capak, P., Garmire, G. P., Hornschemeier, A. E., Steffen, A. T., Wehner, E. H., 2002, AJ, 124, 1839  
 Becker, R. H., White, R. L., Helfand, D. J., 1995, ApJ, 450, 559  
 Brandt, W. N., Laor, A., Wills, B. J., 2000, AJ, 528, 637  
 Brandt, W. N., et al., 2001, AJ, 122, 2810  
 Brinkmann, W., Laurent-Muehleisen, S. A., Voges, W., Siebert, J., Becker, R. H., Brotherton, M. S., White, R. L., Gregg, M. D., 2000, A&A, 356, 462  
 Cash, W., 1979, ApJ, 228, 939  
 Comastri, A., Setti, G., Zamorani, G., Hasinger, G., 1995, A&A, 296, 1  
 Condon, J. J., Cotton, W. D., Greisen, E. W., Yin, Q. F., Perley, R. A., Taylor, G. B., Broderick, J. J., 1998, AJ, 115, 1693  
 Croom, S. M., Smith, R. J., Boyle, B. J., Shanks, T., Loaring, N. S., Miller, L., Lewis, I. J., 2001, MNRAS, 322, L29  
 Dickey, J. M., Lockman, F. J., 1990, ARA&A, 28, 215  
 Elvis, M., Fiore, F., Wilkes, B., McDowell, J., Bechtold, J., 1993, AAS, 25, 1430  
 Feigelson, E. D., Nelson, P. I., 1985, ApJ, 293, 192  
 Fiore, F., 2003, A&A, 409, 79  
 Gallagher, S. C., Brandt, W. N., Laor, A., Elvis, M., Mathur, S., Wills, B. J., Iyomoto, N., 2001, ApJ, 546, 795  
 Gallagher, S. C., Brandt, W. N., Chartas, G., Garmire, G. P., 2002, ApJ, 567, 37  
 Gallagher, S. C., Brandt, W. N., Wills, B. J., Charlton, J. C., Chartas, G., Laor, A., 2004, ApJ, 603, 425  
 Georgakakis, A., Georgantopoulos, I., Stewart, G. C., Shanks, T., Boyle, B. J., 2003, MNRAS, 344, 161  
 Georgakakis, A., Georgantopoulos, I., Vallbe, M., Kolokotronis, V., Basilakos, S., Plionis, M., Stewart, G. C., Shanks, T., Boyle, B. J., 2004, MNRAS, 349, 135  
 Georgantopoulos, I., Georgakakis, A., Stewart, G. C., Akylas, A., Boyle, B. J., Shanks, T., Griffiths, R. E., 2003, 342, 321  
 Georgantopoulos, I., Georgakakis, A., Akylas, A., Stewart, G. C., Giannakis, O., Shanks, T., Kitsionas, S., 2004, MNRAS, in press, astro-ph/0404048  
 Giacconi, R., et al., 2002, ApJS, 139, 369  
 Green, Paul J., Aldcroft, T. L., Mathur, S., Wilkes, B. J., Elvis, M., 2001, ApJ, 558, 109  
 Green, Paul J., et al., 1995, ApJ, 450, 51  
 Hewett, P. C., Foltz, C. B., 2003, AJ, 125, 1784  
 Isobe, T., Feigelson, E. D., Nelson, P. I., 1986, ApJ, 306, 490  
 LaValley, M., Isobe, T., Feigelson, E. D., 1992, in ASP Conf. Ser. 25, Astronomical Data Analysis Software and Systems, ed. D. M. Worrall, C. Biemesderfer, J. Barnes (San Francisco:ASP), 245  
 Mushotzky, R. F., Cowie, L. L., Barger, A. J., Arnaud, K. A., 2000, Nature 404, 459  
 Nandra, K., Pounds, K. A., 1994, MNRAS, 268, 405  
 Norman, C., et al., 2002, ApJ, 571, 218  
 Piconcelli, E., Cappi, M., Bassani, L., Di Cocco, G., Dadina, M., 2003, A&A, 412, 689  
 Reeves, J. N., Turner, M. J. L., 2000, MNRAS, 316, 234  
 Reichard, T. A., et al., 2003, AJ, 126, 2594  
 Risaliti, G., Marconi, A., Maiolino, R., Salvati, M., Severgnini, P., 2001, A&A, 371, 37  
 Schmidt, M., Green, R. F., 1983, ApJ, 269, 352  
 Stern, D., et al., 2002, ApJ, 568, 71  
 Strüder, L., et al., 2001, A&A, 365, L18  
 Turner, M. J., et al., 2001, A&A, 365, L27  
 Vignali, C., Brandt, W. N., Schneider, D. P., 2003a, AJ, 125, 433  
 Vignali, C., Brandt, W. N., Garmire, G. P., Kaspi, S., 2003b, 125, 418  
 Wilkes, B. J., Schmidt, G. D., Cutri, R. M., Ghosh, H., Hines, D. C., Brant, N., Smith, P. S., 2002, ApJ, 564L, 65